Optical rectification and current injection in unbiased semiconductors

F. Nastos and J. E. Sipe
Department of Physics and Institute for Optical Sciences, University of Toronto, 60 St. George Street, Toronto, Ontario, Canada M5S 1A7

(Received 9 August 2010; published 9 December 2010)

We present a full band-structure calculation of the electronic contribution to the second-order susceptibility in the limit of a sum frequency that vanishes. We give a sum-over-states expression for the optical rectification coefficient $\chi_{\mathrm{rect}}(\omega) \equiv \chi_{\mathrm{rect}}(0;\omega,-\omega)$, which includes intraband contributions. Intraband transitions additionally lead to shift and injection currents, which we identify in the total response and separate from the optical rectification. The approach applies to all crystal classes and over a wide range of applied optical frequencies. We apply our results to a full band-structure calculation of the optical rectification, shift current, and injection current susceptibilities for wurtzite CdS and CdSe.

DOI: 10.1103/PhysRevB.82.235204 PACS number(s): 42.70.Mp

I. INTRODUCTION

The optical response of a material is often described by a series of optical susceptibilities characterizing its linear and nonlinear response to the electromagnetic field.[1,2] At the level of the second-order response, different physical processes are associated with the frequency components of the second-order susceptibility tensor $\chi_2(-\omega_\Sigma;\omega_\beta,\omega_\gamma)$, where $\omega_\Sigma=\omega_\beta+\omega_\gamma$ is the sum frequency denoting the Fourier component of the induced polarization. For example, second-harmonic generation (SHG) is described by the component $\chi_2(-2\omega;\omega,\omega)$ and the electro-optic effect by the component $\chi_2(-\omega;\omega,0)$. Optical rectification is often attributed to the component $\chi_2(0;\omega,-\omega)$ but it has been shown that for a clean, cold semiconductor, in the independent particle limit, this frequency component is divergent for $\hbar\omega$ above the band-gap energy.[3]

This physical divergence appearing in the limit $\omega_\beta+\omega_\gamma \rightarrow 0$ must be distinguished from apparent divergences that can occur in some optical susceptibility calculations. Early band-structure calculations of the nonlinear optical response used the minimal coupling Hamiltonian, and seemed to exhibit an unphysical divergence at zero frequency.[4] For the expression for second-harmonic generation it was shown that this divergence could be eliminated with the use of appropriate sum rules that connect interband and intraband matrix elements.[4,5] A calculation using the dipole Hamiltonian, rather than the minimal coupling Hamiltonian, eliminates the appearance of unphysical divergences for any frequency components, without the necessity of identifying sum rules. Such a calculation is based on an approach relying on Blount's discussion of the position operator in periodic systems.[6] The remaining *physical* divergences appearing in the rectification limit can be identified with "shift current"[7–12] and "injection current"[13–17] effects, and the finite part of $\chi_2(0;\omega,-\omega)$ can be interpreted as the optical rectification tensor.[3,18–23]

For zinc-blende crystals we have previously shown how the rectification and shift current contributions of the general $\chi_2(-\omega_\Sigma;\omega_\alpha,\omega_\beta)$ susceptibility can be identified for $\omega_\Sigma \approx 0$. In these crystals the injection current vanishes. In this paper we generalize the approach to arbitrary crystal classes. We extract the injection current, shift current, and optical rectification susceptibilities from the general $\chi_2(-\omega_\Sigma;\omega_\alpha,\omega_\beta)$ susceptibility tensor. We provide sample calculations of the response for wurtzite CdSe and CdS using a full potential linearized augmented plane wave (FLAPW) band-structure scheme, together with the LDA plus a "scissors approximation," to evaluate our expressions. Among those crystal structures that exhibit all three effects of optical rectification, shift, and injection current, the wurtzite structure is one of the simplest. These three effects, however, do not comprise the entire second order response for pulsed excitation, even in the independent particle approximation. In the ultrafast regime, there are also currents arising from the dispersion of $\chi_2(-\omega_\Sigma;\omega_\alpha,\omega_\beta)$. These currents are typically weaker than the shift, injection, and rectification currents appearing in the dc limit but they are still captured in our framework.

While there is a lack of extensive experimental data of these effects in wurtzite crystals, recent experiments investigating the terahertz (THz) emission from CdSe and CdS samples optically excited above the band gap have been reported by Laman *et al.*,[13] in which the THz emission was attributed to shift and injection current processes. From their measurements, they were able to back out estimates for the shift and injection susceptibility tensors. We will compare our results to theirs where possible, and our optical rectification susceptibility calculations to the low-frequency values of other second order nonlinear optical susceptibilities for CdSe.

This paper is outlined as follows. Section II extends our earlier derivations, and demonstrates how the second-order optical response tensor in the independent particle limit breaks up into optical rectification, shift current, and injection current contributions. The notation refers heavily to Sipe and Shkrebtii[18] and Nastos and Sipe.[19] In Sec. III we present numerical calculations of these contributions for wurtzite CdSe and compare, where possible, to experimental findings. We conclude in Sec. IV.

II. THEORY

We follow the notation laid out in Nastos and Sipe,[19] and Sipe and Shkrebtii.[18] In the independent particle approxima-

tion, the second-order response tensor is given by

$$\chi_2^{abc}(-\omega_\Sigma;\omega_\beta,\omega_\gamma)=\chi_{2\text{inter}}^{abc}(-\omega_\Sigma;\omega_\beta,\omega_\gamma)+\frac{\bar{\sigma}_2^{abc}(-\omega_\Sigma;\omega_\beta,\omega_\gamma)}{(-i\omega_\Sigma)}+\frac{\bar{K}_2^{abc}(-\omega_\Sigma;\omega_\beta,\omega_\gamma)}{(-i\omega_\Sigma)^2}, \quad (1)$$

where $\omega_\Sigma=\omega_\beta+\omega_\gamma$, which explicitly shows the divergences as $\omega_\Sigma\to 0$. Roman superscripts denote Cartesian coordinates. The first two terms on the right-hand side of Eq. (1) have different divergences in ω_Σ and correspond to electric currents and dipole polarizations injected into the crystal that have different temporal behavior under pulsed excitation. The three tensors $\bar{K}^{abc}$, $\bar{\sigma}_2^{abc}$, and $\chi_{2\text{inter}}^{abc}$ were introduced in Sipe and Shkrebtii,[18] and shown to be nondivergent for all ω_β and ω_γ.

In Nastos and Sipe[19] we discussed the response in the limit of continuous wave excitation from linearly polarized light. Here we generalize to arbitrary polarization, and write the pulsed field as

$$\mathbf{E}(t)=\mathbf{E}_{\text{env}}(t)e^{-i\omega_0 t}+\mathbf{E}_{\text{env}}^*(t)e^{i\omega_0 t}. \quad (2)$$

The envelope function $\mathbf{E}_{\text{env}}(t)$ can be complex in general to allow for circular polarized light. Much of the following discussion will be about the response to circularly polarized excitation.

The electric polarization is often written in terms of the susceptibility tensor and electric field,[24]

$$P^a(t)=\int\frac{d\omega_\beta}{2\pi}\int\frac{d\omega_\gamma}{2\pi}\chi_2^{abc}(-\omega_\Sigma;\omega_\beta,\omega_\gamma)E^b(\omega_\beta)E^c(\omega_\gamma)e^{-i\omega_\Sigma t}, \quad (3)$$

where

$$\mathbf{E}(\omega)=\int dt\mathbf{E}(t)e^{i\omega t} \quad (4)$$

is the Fourier transform of $\mathbf{E}(t)$. But this clearly leads to a divergent polarization, at least within the context of optically generated currents, and so we focus on the current $\langle\mathbf{J}\rangle=d\mathbf{P}/dt$. Each of the three terms in the right-hand side of Eq. (1) gives rise to an individual contribution to the total current response

$$\langle\mathbf{J}\rangle=\langle\mathbf{J}_{\text{inter}}\rangle+\langle\mathbf{J}_{\text{intra}}\rangle^{\text{I}}+\langle\mathbf{J}_{\text{intra}}\rangle^{\text{II}}. \quad (5)$$

Taking the appropriate time derivatives of the polarization Eq. (3) in order to bring down factors of $-i\omega_\Sigma$ and get well-behaved expressions, the first of these terms is explicitly given by $\langle\mathbf{J}_{\text{inter}}\rangle=d\langle\mathbf{P}\rangle_{\text{inter}}/dt$, where

$$\langle P_{\text{inter}}^a(t)\rangle=\int\frac{d\omega_\beta}{2\pi}\int\frac{d\omega_\gamma}{2\pi}\chi_{2\text{inter}}^{abc}(-\omega_\Sigma;\omega_\beta,\omega_\gamma)\times E^b(\omega_\beta)E^c(\omega_\gamma)e^{-i\omega_\Sigma t}, \quad (6)$$

the second by

$$\langle J_{\text{intra}}^a(t)\rangle^{\text{I}}=\int\frac{d\omega_\beta}{2\pi}\int\frac{d\omega_\gamma}{2\pi}\bar{\sigma}_2^{abc}(-\omega_\Sigma;\omega_\beta,\omega_\gamma)\times E^b(\omega_\beta)E^c(\omega_\gamma)e^{-i\omega_\Sigma t}, \quad (7)$$

and the third by

$$\frac{d}{dt}\langle J_{\text{intra}}^a(t)\rangle^{\text{II}}=\int\frac{d\omega_\beta}{2\pi}\int\frac{d\omega_\gamma}{2\pi}\bar{K}^{abc}(-\omega_\Sigma;\omega_\beta,\omega_\gamma)\times E^b(\omega_\beta)E^c(\omega_\gamma)e^{-i\omega_\Sigma t}. \quad (8)$$

In Nastos and Sipe[19] we focused on GaAs and GaP, and limited the treatment of $\langle J_{\text{intra}}^a(t)\rangle^{\text{I}}$ and $d\langle J_{\text{intra}}^a(t)\rangle^{\text{II}}/dt$ to zinc-blende crystals. Here we generalize the development to arbitrary crystal classes.

To isolate the nondispersive contributions, we expand the electric field product $E^b(\omega_\beta)E^c(\omega_\gamma)$ as

$$E^b(\omega_\beta)E^c(\omega_\gamma)=[E^b(\omega_\beta)E^c(\omega_\gamma)]_{\text{THz}}+[E^b(\omega_\beta)E^c(\omega_\gamma)]_{\text{SHG}}, \quad (9)$$

where we define

$$[E^b(\omega_\beta)E^c(\omega_\gamma)]_{\text{THz}}\equiv E_{\text{env}}^b(\omega_\beta-\omega_0)E_{\text{env}}^{c*}(-\omega_\gamma-\omega_0)+E_{\text{env}}^{b*}(-\omega_\beta-\omega_0)E_{\text{env}}^c(\omega_\gamma-\omega_0) \quad (10)$$

and

$$[E^b(\omega_\beta)E^c(\omega_\gamma)]_{\text{SHG}}\equiv E_{\text{env}}^b(\omega_\beta-\omega_0)E_{\text{env}}^c(\omega_\gamma-\omega_0)+E_{\text{env}}^{b*}(-\omega_\beta-\omega_0)E_{\text{env}}^{c*}(-\omega_\gamma-\omega_0). \quad (11)$$

Here $E_{\text{env}}^{b*}(\omega)\equiv[E_{\text{env}}^b(\omega)]^*$ refers to the complex conjugate of the Fourier transform of the envelope function (as opposed to the Fourier transform of the complex conjugate of the envelope function). Our focus is on the limit $\omega_\beta\approx-\omega_\gamma$ so we consider the slowly varying response, and keep only the term $[E^b(\omega_\beta)E^c(\omega_\gamma)]_{\text{THz}}$.

We now substitute Eqs. (9) and (10) into the total response given by Eqs. (6)–(8). Using the intrinsic symmetry[1] properties of $\chi_2^{abc}(-\omega_\Sigma;\omega_\beta,\omega_\gamma)$, we find from Eq. (6),

$$\langle P_{\text{inter}}^a(t)\rangle=2\int\frac{d\Omega_\beta}{2\pi}\int\frac{d\Omega_\gamma}{2\pi}\chi_{2\text{inter}}^{abc}(-\Omega_\Sigma;\omega_0+\Omega_\beta,-\omega_0+\Omega_\gamma)E_{\text{env}}^b(\Omega_\beta)E_{\text{env}}^{c*}(-\Omega_\gamma)e^{-i\Omega_\Sigma t}, \quad (12)$$

where Ω_β and Ω_γ are new dummy variables introduced so that the zero-frequency components of E_{env}^b and E_{env}^c correspond to $\Omega_\beta=\Omega_\gamma=0$; the factor of 2 arises from the two terms appearing in Eq. (10). Since $\bar{\sigma}_2^{abc}$ and $\bar{K}^{abc}$ also satisfy intrinsic permutation symmetry,[18] we have

$$\langle J_{\text{intra}}^a(t)\rangle^{\text{I}}=2\int\frac{d\Omega_\beta}{2\pi}\int\frac{d\Omega_\gamma}{2\pi}\bar{\sigma}_2^{abc}(-\Omega_\Sigma;\omega_0+\Omega_\beta,-\omega_0+\Omega_\gamma)E_{\text{env}}^b(\Omega_\beta)E_{\text{env}}^{c*}(-\Omega_\gamma)e^{-i\Omega_\Sigma t} \quad (13)$$

from Eq. (7), and

$$\frac{d}{dt}\langle J^a_{\text{intra}}(t)\rangle^{\text{II}} = 2\int \frac{d\Omega_\beta}{2\pi}\int \frac{d\Omega_\gamma}{2\pi}\bar{K}^{abc}(-\Omega_\Sigma;\omega_0+\Omega_\beta,-\omega_0+\Omega_\gamma)E^b_{\text{env}}(\Omega_\beta)E^{c*}_{\text{env}}(-\Omega_\gamma)e^{-i\Omega_\Sigma t} \tag{14}$$

from Eq. (8).

The expressions (12)–(14) often do not provide the most transparent physical description of the response. As discussed in Nastos and Supe,[19] one can cleanly introduce the definition of shift and injection currents in addition to the optical rectification. It is often more physically appealing to describe the second-order response in terms of these effects since a microscopic mechanism can be associated with each one.[18]

From Eqs. (12)–(14) we identify the injection current as a current rate that follows the pulse intensity. The susceptibility tensor describing the injection current, which we denote by $\eta^{abc}_{\text{inj}}(\omega)$, can be obtained from the limit

$$\eta^{abc}_{\text{inj}}(\omega_0) \equiv \lim_{\Omega_\Sigma\to 0}(-i\Omega_\Sigma)^2\chi^{abc}_2(-\omega_\Sigma;\omega_0+\Omega_\beta,-\omega_0+\Omega_\gamma). \tag{15}$$

The limit here refers to taking $\Omega_\beta\to 0$ and $\Omega_\gamma\to 0$ in either order.

The shift current is an induced current that follows the pulse intensity. Subtracting the singular term $\eta^{abc}_{\text{inj}}(\omega_0)/(-i\Omega^2_\Sigma)$ from $\chi^{abc}_2(-\Omega_\Sigma;\omega_\beta,\omega_\gamma)$, the tensor $\sigma^{abc}_{\text{shift}}(\omega)$ describing shift current can be obtained from the limit

$$\sigma^{abc}_{\text{shift}}(\omega_0) \equiv \lim_{\Omega_\Sigma\to 0}(-i\Omega_\Sigma)\left[\chi^{abc}_2(-\Omega_\Sigma;\omega_0+\Omega_\beta,-\omega_0+\Omega_\gamma) - \frac{\eta^{abc}_{\text{inj}}(\omega_0)}{(-i\Omega_\Sigma)^2}\right]. \tag{16}$$

The optical rectification is an induced polarization that follows the pulse intensity, and its susceptibility tensor $\chi^{abc}_{\text{rect}}(\omega)\equiv\chi^{abc}_{\text{rect}}(0;\omega,-\omega)$ can be obtained by subtracting the singular contributions of shift and injection current from Eq. (1) and then taking the limit $\omega_\Sigma\to 0$, so that

$$\chi^{abc}_{\text{rect}}(\omega_0) \equiv \lim_{\Omega_\Sigma\to 0}\left[\chi^{abc}_2(-\Omega_\Sigma;\omega_0+\omega_\beta,-\omega_0+\omega_\gamma) - \frac{\sigma^{abc}_{\text{shift}}(\omega_0)}{(-i\Omega_\Sigma)} - \frac{\eta^{abc}_{\text{inj}}(\omega_0)}{(-i\Omega_\Sigma)^2}\right]. \tag{17}$$

This prescription extracts the different effects that occur in the independent particle limit, and classifies them according to their microscopic origin and phenomenological description. We bundle the remaining terms of χ^{abc}_2 into $\chi^{abc}_{2\text{rem}}$, given formally by the difference

$$\chi^{abc}_{2\text{rem}}(-\Omega_\Sigma;\omega_0+\Omega_\beta,-\omega_0+\Omega_\gamma) \equiv \chi^{abc}_2(-\Omega_\Sigma;\omega_0+\Omega_\beta,-\omega_0+\Omega_\gamma) - \chi^{abc}_{\text{rect}}(\omega_0) - \frac{\sigma^{abc}_{\text{shift}}(\omega_0)}{(-i\Omega_\Sigma)} - \frac{\eta^{abc}_{\text{inj}}(\omega_0)}{(-i\Omega_\Sigma)^2}. \tag{18}$$

This quantity $\chi^{abc}_{2\text{rem}}$ accounts for the dispersive effects in the low-frequency response, and vanishes in the continuous wave limit.

To identify the equations for each of the limiting terms of Eqs. (15)–(18) we consider the total response at the level of $d\langle J^a\rangle/dt$, expand it in powers of Ω_β and Ω_γ, and identify terms with the appropriate power of Ω_Σ for each physical effect.

This approach has one further aim. While previously given equations[18] for $\bar{K}^{abc}$, $\bar{\sigma}^{abc}_2$, and $\chi^{abc}_{2\text{inter}}$ can be used directly to evaluate the response, this can be computationally expensive since it requires calculating and storing the susceptibility tensors for all pairs of frequencies Ω_β and Ω_γ spanned by the pulse. Below, we write the response tensors in terms of effective single-frequency tensors, which greatly simplifies the computations required to evaluate the total response.

We first consider the sum $d\langle J^a(t)\rangle/dt = d^2\langle P^a_{\text{inter}}\rangle/dt^2 + d\langle J^a_{\text{intra}}(t)\rangle^{\text{I}}/dt + d\langle J^a_{\text{intra}}(t)\rangle^{\text{II}}/dt$,

$$\frac{d}{dt}\langle J^a(t)\rangle = 2\int \frac{d\Omega_\beta}{2\pi}\int \frac{d\Omega_\gamma}{2\pi}E^b_{\text{env}}(\Omega_\beta)E^{c*}_{\text{env}}(-\Omega_\gamma)e^{-i\Omega_\Sigma t} \times[(-i\Omega_\Sigma)^2\chi^{abc}_{2\text{inter}}(-\Omega_\Sigma;\omega_0+\Omega_\beta,-\omega_0+\Omega_\gamma) + T^{abc}(-\Omega_\Sigma;\omega_0+\Omega_\beta,-\omega_0+\Omega_\gamma)], \tag{19}$$

where T^{abc} is defined from Eqs. (13) and (14) as

$$T^{abc}(-\Omega_\Sigma;\omega_0+\Omega_\beta,-\omega_0+\Omega_\gamma) \equiv (-i\Omega_\Sigma)\bar{\sigma}^{abc}_2(-\Omega_\Sigma;\omega_0+\Omega_\beta,-\omega_0+\Omega_\gamma) + \bar{K}^{abc}(-\Omega_\Sigma;\omega_0+\Omega_\beta,-\omega_0+\Omega_\gamma). \tag{20}$$

The tensors $\bar{\sigma}^{abc}_2$ and $\bar{K}^{abc}_2$ can be expressed in terms of single-frequency tensors,[19] so that

$$\bar{\sigma}^{abc}_2(-\omega_\Sigma;\omega_\beta,\omega_\gamma) = -i[\Lambda^{abc}(\omega_\beta)+\Lambda^{acb}(\omega_\gamma)] \tag{21}$$

and

$$\bar{K}^{abc}(-\omega_\Sigma;\omega_\beta,\omega_\gamma) = \Gamma^{abc}(\omega_\beta)-\Gamma^{abc}(\omega_\gamma), \tag{22}$$

where $\Lambda^{abc}(\omega)$ and $\Gamma^{abc}(\omega)$ are effective single-frequency tensors, with real and imaginary parts that are related by the Kramers-Kronig relations. We denote the real part with subscript I and the imaginary parts with subscript II, so that $\Lambda^{abc}(\omega)=\Lambda^{abc}_{\text{I}}(\omega)+i\Lambda^{abc}_{\text{II}}(\omega)$ and $\Gamma^{abc}(\omega)=\Gamma^{abc}_{\text{I}}(\omega)+i\Gamma^{abc}_{\text{II}}(\omega)$. From the symmetry properties[19] of the real and imaginary parts of $\Lambda^{abc}(\omega)$ and $\Gamma^{abc}(\omega)$, T^{abc} can be written in terms of real and imaginary parts: $T^{abc}=T^{abc}_{\text{I}}+iT^{abc}_{\text{II}}$, where the imaginary part T^{abc}_{II} is strictly zero below the band gap.

Now we Taylor expand T^{abc} in Eq. (19) in order to identify the different powers of $(-i\Omega_\Sigma)$ in Eqs. (15)–(17). Expanding $\Lambda^{abc}(\omega)$ and $\Gamma^{abc}(\omega)$ about the carrier frequency ω_0, the real part of T^{abc} is

$$T^{abc}_{\text{I}}(-\Omega_\Sigma;\omega_0+\Omega_\beta,-\omega_0\Omega_\gamma) \approx -\Omega_\Sigma[\Lambda^{abc}_{\text{I}}(\omega_0)+\Omega_\beta\Lambda^{abc'}_{\text{I}}(\omega_0)-\Lambda^{acb}_{\text{I}}(\omega_0) + \Omega_\gamma\Lambda^{acb'}_{\text{I}}(\omega_0)]+\Omega_\Sigma\Gamma^{abc'}_{\text{I}}(\omega_0)+\frac{1}{2}\Omega_\Sigma(\Omega_\beta$$

$$-\Omega_\gamma)\Gamma_{\mathrm{I}}^{abc''}(\omega_0), \tag{23}$$

where we have dropped terms of order $\mathcal{O}(\Omega^3/\omega_0^3)$ and higher. In Eq. (23) and below we use primes to denote derivatives with respect to ω, e.g.,

$$\Gamma_{\mathrm{I}}^{abc'}(\omega_0) \equiv \left[\frac{d\Gamma_{\mathrm{I}}(\omega)}{d\omega}\right]_{\omega=\omega_0}, \tag{24}$$

$$\Gamma_{\mathrm{I}}^{abc''}(\omega_0) \equiv \left[\frac{d^2\Gamma_{\mathrm{I}}(\omega)}{d\omega^2}\right]_{\omega=\omega_0}, \tag{25}$$

etc. We can further simplify Eq. (23) by using

$$\Gamma^{abc'}(\omega) = \Lambda^{abc}(\omega) - \Lambda^{acb}(\omega), \tag{26}$$

which we derive in the Appendix. Using this gives

$$T_{\mathrm{I}}^{abc}(-\Omega_\Sigma;\omega_0+\Omega_\beta,-\omega_0+\Omega_\gamma) = (-i\Omega_\Sigma)^2\frac{1}{2}[\Lambda_{\mathrm{I}}^{abc'}(\omega_0)+\Lambda_{\mathrm{I}}^{acb'}(\omega_0)]. \tag{27}$$

The imaginary part iT_{II}^{abc} can be written as

$$\begin{aligned} iT_{\mathrm{II}}^{abc}(-\Omega_\Sigma;\omega_0+\Omega_\beta,-\omega_0+\Omega_\gamma) &= +2i\Gamma_{\mathrm{II}}^{abc}(\omega_0) - i\Omega_\Sigma[\Lambda_{\mathrm{II}}^{abc}(\omega_0)+\Lambda_{\mathrm{II}}^{acb}(\omega_0)] \\ &+ i(\Omega_\beta-\Omega_\gamma)\Gamma_{\mathrm{II}}^{abc'}(\omega_0) + \frac{i}{2}(\Omega_\gamma^2-\Omega_\beta^2)[\Lambda_{\mathrm{II}}^{abc'}(\omega_0) \\ &+ \Lambda_{\mathrm{II}}^{acb'}(\omega_0)] - \frac{i}{2}(\Omega_\beta\Omega_\gamma)\Gamma_{\mathrm{II}}^{abc''}(\omega_0), \end{aligned} \tag{28}$$

where we have dropped terms of order (Ω^3/ω).

We are now in a position to identify the injection current susceptibility tensor. Using Eq. (28) in Eq. (19), we see that the first term in Eq. (28), $2i\Gamma_{\mathrm{II}}^{abc}(\omega)$, is independent of Ω_β and Ω_γ, and thus it gives a current-injection rate that is proportional to the intensity. This term then is the injection current susceptibility $\eta_{\mathrm{inj}}^{abc}(\omega)$, and we have

$$\eta_{\mathrm{inj}}^{abc}(\omega) = 2i\Gamma_{\mathrm{II}}^{abc}(\omega). \tag{29}$$

The injection current rate is the continuous wave limit of Eq. (14), given by

$$\dot{J}_{\mathrm{inj}}^a = 2i\,\eta_{\mathrm{inj}}^{abc}(\omega_0)\mathrm{Im}[E_{\mathrm{env}}^b(t)E_{\mathrm{env}}^{c*}(t)]. \tag{30}$$

The expression for $\Gamma_{\mathrm{II}}^{abc}(\omega)$ is[18]

$$\Gamma_{\mathrm{II}}^{abc}(\omega) = -\frac{ie^3\pi}{4\hbar^2}\int\frac{d^3k}{8\pi^3}\sum_{mn}\Delta_{mn}^a[r_{mn}^c,r_{mn}^b]f_{nm}\delta(\omega_{mn}-\omega). \tag{31}$$

The quantity $f_{nm}=f_n-f_m$ where f_n is the ground-state occupation number for band n, $r_{mn}^a(\mathbf{k})$ is the interband position matrix element, $\omega_{mn}(\mathbf{k})=\omega_m(\mathbf{k})-\omega_n(\mathbf{k})$, where $\hbar\omega_m(\mathbf{k})$ is the band-structure energy of band m at $\mathbf{k}$, and $\Delta_{mn}^c \equiv v_{mm}^c(\mathbf{k}) - v_{nn}^c(\mathbf{k})$, where $v_{mm}^c(\mathbf{k})=d\omega_m(\mathbf{k})/dk^c$ is the group velocity. We have dropped the explicit $\mathbf{k}$ label in Eq. (31).

The shift current can be found from the second term of Eq. (28), $-i\Omega_\Sigma[\Lambda_{\mathrm{II}}^{abc}(\omega_0)+\Lambda_{\mathrm{II}}^{acb}(\omega_0)]$. The factor $-i\Omega_\Sigma$ indicates that the current from this term follows the pulse intensity, as phenomenologically expected of the shift current. From Eqs. (16), (19), and (21) we have

$$\sigma_{\mathrm{shift}}^{abc}(\omega) = \Lambda_{\mathrm{II}}^{abc}(\omega) + \Lambda_{\mathrm{II}}^{acb}(\omega). \tag{32}$$

The shift current is then given by

$$J_{\mathrm{shift}}^a = 2\sigma_{\mathrm{shift}}^{abc}(\omega_0)\mathrm{Re}[E_{\mathrm{env}}^b(t)E_{\mathrm{env}}^{c*}(t)]. \tag{33}$$

The expression for the $\Lambda_{\mathrm{II}}^{abc}(\omega)$ is

$$\Lambda_{\mathrm{II}}^{abc}(\omega) = -\frac{ie^3\pi}{2\hbar^2}\int\frac{d^3k}{8\pi^3}f_{nm}\sum_{nm}r_{mn}^b r_{nm;a}^c\delta(\omega_{mn}-\omega). \tag{34}$$

We now identify the optical rectification. We see that no term in iT_{II}^{abc} has a leading factor of Ω_Σ^2 and so there is no contribution from iT_{II}^{abc} to a polarization that follows the optical pulse, and thus no contribution to optical rectification. Since $\chi_{\mathrm{2inter}}^{abc}(-\omega_\Sigma;\omega_\beta,\omega_\gamma)$ is nondivergent, the term $\chi_{\mathrm{2inter}}^{abc}(0;\omega_0,-\omega_0)$ does contribute to $\chi_{\mathrm{rect}}^{abc}(\omega_0)$. Corrections to $\chi_{\mathrm{2inter}}^{abc}(0;\omega_0,-\omega_0)$, from expanding $\chi_{\mathrm{2inter}}^{abc}(-\Omega_\Sigma;\omega_0+\Omega_\beta,-\omega_0+\Omega_\gamma)$ about $\Omega_\beta=0$ and $\Omega_\gamma=0$, give dispersive terms that describe an induced polarization that depends on time derivatives of the envelope function of the laser field.

However, $\chi_{\mathrm{2inter}}^{abc}(0;\omega_0,-\omega_0)$ is not the only term contributing to the optical rectification. Because of the factor $(-i\Omega_\Sigma)^2$ in $T_{\mathrm{I}}^{abc}(-\Omega_\Sigma;\omega_0+\Omega_\beta,-\omega_0+\Omega_\gamma)$ [Eq. (27)], the electronic response associated with the factor $\frac{1}{2}[\Lambda_{\mathrm{I}}^{abc'}(\omega_0)+\Lambda_{\mathrm{I}}^{acb'}(\omega_0)]$ is treated at the same level of $\chi_{\mathrm{2inter}}^{abc}(0;\omega_0;-\omega_0)$ and is part of the optical rectification tensor $\chi_{\mathrm{rect}}^{abc}(\omega_0)$. Using Eqs. (17) and (27) gives our general result for the optical rectification tensor

$$\chi_{\mathrm{rect}}^{abc}(\omega) = \chi_{\mathrm{2inter}}^{abc}(0;\omega;-\omega) + \frac{1}{2}[\Lambda_{\mathrm{I}}^{abc'}(\omega)+\Lambda_{\mathrm{I}}^{acb'}(\omega)]. \tag{35}$$

The optical rectification polarization is given by

$$P_{\mathrm{rect}}(t) = 2\chi_{\mathrm{rect}}^{abc}(\omega_0)E_{\mathrm{env}}^b(t)E_{\mathrm{env}}^{c*}(t). \tag{36}$$

The reality of $P_{\mathrm{rect}}(t)$ is ensured by the relation $\chi_{\mathrm{rect}}^{abc}(\omega_0)=\chi_{\mathrm{rect}}^{acb*}(\omega_0)$.

To obtain the formula for $\chi_{\mathrm{rect}}^{abc}(\omega)$, the formula for $\chi_{\mathrm{2inter}}^{abc}(\omega)$ can be obtained from Sipe and Shkrebtii[18] and Nastos and Sipe.[19] There is was shown that $\chi_{\mathrm{2inter}}^{abc}(\omega)$ is given by

$$\chi_{\mathrm{2inter}}^{abc}(\omega) = B^{abc}(\omega) + B^{acb*}(\omega), \tag{37}$$

where the imaginary part of $B^{abc}(\omega)$, denoted by $B_{\mathrm{II}}^{abc}(\omega)$, is given by

$$B_{\mathrm{II}}^{abc}(\omega) = \frac{e^3\pi}{2\hbar^2}\int\frac{d^3k}{8\pi^3}\sum_{nmp}f_{nm}\delta(\omega-\omega_{mn})\left[r_{nm}^b\left(\frac{r_{mp}^a r_{pn}^c}{\omega_{pm}} + \frac{r_{mp}^c r_{pn}^a}{\omega_{pn}}\right) + \frac{ir_{nm}^a r_{mn}^b\Delta_{mn}^c}{\omega_{mn}^2} + \frac{ir_{nm}^c r_{mn;b}^a}{\omega_{mn}}\right]. \tag{38}$$

The quantity $r_{mn;b}^a(\mathbf{k})$ is the generalized derivative of the interband matrix element $r_{mn}^a(\mathbf{k})$. The reader is referred to Sipe and Shkrebtii[18] and Natsos and Sipe.[19] for more details on

the generalized derivative and the evaluation of such quantities. The real part $B_{\mathrm{I}}^{abc}(\omega)$ can then be found by using the Kramers-Kronig relation. The remaining term in $\chi_{\mathrm{rect}}^{abc}(\omega)$, which is $\frac{1}{2}[\Lambda_{\mathrm{I}}^{abc'}(\omega)+\Lambda_{\mathrm{I}}^{acb'}(\omega)]$, can be determined by first calculating the imaginary part of $\Lambda^{abc}(\omega)$, and then evaluating $\Lambda_{\mathrm{I}}^{abc}(\omega)$ with the second Kramers-Kronig relation (see Ref. 19 for details). The derivative $\Lambda_{\mathrm{I}}^{abc'}(\omega)$ can be determined with finite difference. Note that while both the real and imaginary parts of $B^{abc}(\omega)$ are contained in the expression for $\chi_{\mathrm{rect}}^{abc}(\omega)$, only the real part of $\Lambda^{abc}(\omega)$ appears.

Formally then, the remaining dispersive terms can be written as

$$\begin{aligned}\chi_{2\mathrm{rem}}^{abc}(-\Omega_\Sigma;\omega_0+\Omega_\beta,-\omega_0+\Omega_\gamma)&\equiv\chi_{2\mathrm{inter}}^{abc}(-\Omega_\Sigma;\omega_0+\Omega_\beta,-\omega_0+\Omega_\gamma)\\&+\frac{T^{abc}(-\Omega_\Sigma;\omega_0+\Omega_\beta,-\omega_0+\Omega_\gamma)}{(-i\Omega_\Sigma)^2}\\&-\chi_{\mathrm{rect}}^{abc}(\omega_0)-\frac{\sigma_{\mathrm{shift}}^{abc}(\omega_0)}{(-i\Omega_\Sigma)}-\frac{\eta_{\mathrm{inj}}^{abc}(\omega_0)}{(-i\Omega_\Sigma)^2}.\end{aligned}\tag{39}$$

Dispersive terms arising from $\chi_{2\mathrm{inter}}^{abc}$ give the usual types of dispersion effects one would normally expect from expanding $\chi_{2\mathrm{inter}}^{abc}(-\Omega_\Sigma;\omega_0+\Omega_\beta,-\omega_0+\Omega_\gamma)$ about the carrier frequency. However, the three remaining terms in Eq. (28), which we have not addressed yet, are susceptibility tensors for currents that do not fit into the framework of dividing the second-order response into rectification, shift, and injection currents. We label these remaining three currents $J_1^a(t)$, $J_2^a(t)$, and $J_3^a(t)$, respectively. They arise from the dispersion in χ_{rem}, given by Eq. (18), exist only for excitation above the band gap, and vanish in the continuous-wave limit. They depend on derivatives of the electric field envelope function, and cannot be written in terms of simple derivatives of only the intensity envelope function. While the focus of this paper is on the nondispersive effect of optical rectification, shift, and injection current, for completeness we conclude this section by giving the electric field dependence of these dispersive currents.

The term, $i(\Omega_\beta-\Omega_\gamma)\Gamma_{\mathrm{II}}^{abc'}(\omega_0)$, in Eq. (28), results in a current rate $\frac{d}{dt}\langle J_1^a(t)\rangle$ given by

$$\frac{d}{dt}\langle J_1^a(t)\rangle=2\Gamma_{\mathrm{II}}^{abc'}(\omega_0)\left[E_{\mathrm{env}}^b(t)\frac{d}{dt}E_{\mathrm{env}}^{c*}(t)-E_{\mathrm{env}}^{c*}(t)\frac{d}{dt}E_{\mathrm{env}}^b(t)\right].\tag{40}$$

Using the antisymmetry of $\Gamma^{abc}(\omega)$ under exchange of b and c, it is straightforward to show that if the electric field has a fixed polarization, so that up to a time-independent phase the amplitudes of orthogonal field components are the same, then $d\langle J_1^a(t)\rangle/dt$ vanishes. It does not vanish, however, if the electric field polarization is changing with respect to time.

The next term in Eq. (28) is $\frac{i}{2}(\Omega_\gamma^2-\Omega_\beta^2)[\Lambda_{\mathrm{II}}^{abc'}(\omega_0)+\Lambda_{\mathrm{II}}^{acb'}(\omega_0)]$. This gives a current rate $d\langle J_2^a(t)\rangle/dt$ given by

$$\frac{d}{dt}\langle J_2^a(t)\rangle=i[\Lambda_{\mathrm{II}}^{abc'}(\omega_0)+\Lambda_{\mathrm{II}}^{acb'}(\omega_0)]\times\left[E_{\mathrm{env}}^{b*}(t)\frac{d^2}{dt^2}E_{\mathrm{env}}^c(t)-E_{\mathrm{env}}^b(t)\frac{d^2}{dt^2}E_{\mathrm{env}}^{c*}(t)\right].\tag{41}$$

In most cases of interest this term also vanishes. It survives when the electric field carries a time-dependent phase.

The last term in Eq. (28) is $-i\frac{1}{2}(\Omega_\beta\Omega_\gamma)\Gamma_{\mathrm{II}}^{abc''}(\omega_0)$. Associated with it is a current rate $d\langle J_3^a(t)\rangle/dt$, given by

$$\frac{d}{dt}\langle J_3^a(t)\rangle=i\frac{1}{2}\Gamma_{\mathrm{II}}^{abc''}(\omega)\left[\frac{d}{dt}E_{\mathrm{env}}^b(t)\frac{d}{dt}E_{\mathrm{env}}^{c*}(t)-\frac{d}{dt}E_{\mathrm{env}}^{b*}(t)\frac{d}{dt}E_{\mathrm{env}}^c(t)\right].\tag{42}$$

Unlike the two terms J_1 and J_2, this term does not necessarily vanish when the electric field is circular polarized, although it does vanish for linear polarizations. To see that it does not vanish, consider a crystal oriented so that the tensor component $\Gamma_{\mathrm{II}}^{xxz}$ is accessed under normal incidence. If the field is circularly polarized in the crystal, such that $E_{\mathrm{env}}^z(t)=iE_{\mathrm{env}}^x(t)$ then we find

$$\frac{d}{dt}\langle J_3^x(t)\rangle=2\Gamma_{\mathrm{II}}^{xxz''}(\omega)\left|\frac{d}{dt}E_{\mathrm{env}}^x(t)\right|^2.\tag{43}$$

To summarize, the total current response to pulsed excitation is given by $\langle J\rangle$ in Eq. (5). One approach to calculating the total response is to solve directly the three susceptibilities $\chi_{2\mathrm{inter}}$, $\bar{\sigma}_2$, and $\bar{K}$ in Eqs. (12)–(14) from the expressions given in Sipe and Shkrebtii[18] or Nastos and Sipe.[19] A more physically transparent approach is to identify in the expressions (12)–(14) the effects of optical rectification, shift current and injection current. The optical rectification is given by Eqs. (35) and (36), the shift current is given by Eqs. (32) and (33), and the injection current by Eqs. (29) and (30). Within the approximations made in this work, the three effects of optical rectification, shift, and injection current are the only electronic effects existing in the continuous wave limit. What remains in Eqs. (12)–(14) are the dispersive contributions the response.

In addition to the temporal dependence of the typical dispersive terms one would expect from an expansion of the nonlinear susceptibility around the carrier frequency of the pulse, we have identified terms with a more specific temporal dependence, existing only for excitation at photon energies above the band-gap energy and arising from the dispersion of $\bar{\sigma}_2$ and $\bar{K}$. The currents from these terms are specified in J_1, J_2, and J_3 in Eqs. (40)–(42), respectively.

III. WURTZITE CDS AND CDSE

A. Symmetries of the optical response components

We now turn to the numerical evaluation of the response. The dispersive terms J_1, J_2, and J_3 are only significant for very short pulses, typically under 10 fs in duration.[19] Non-

linear optical experiments do not regularly approach that regime, and to our knowledge even the rectification response of GaAs has yet to be experimentally studied on such time scales. For that reason we focus only on the susceptibility calculations of shift current $\sigma^{abc}_{\rm shift}(\omega)$, injection current $\eta^{abc}_{\rm inj}(\omega)$ and optical rectification $\chi^{abc}_{\rm rect}(\omega)$, for which a number of experiments have been reported.

We choose to evaluate these tensors for wurtzite CdS and CdSe since these are two of the simpler bulk semiconductors for which $\eta^{abc}_{\rm inj}(\omega)$ does not vanish. In Ref. 19, we evaluated $\chi^{abc}_{\rm rect}(\omega)$ and $\sigma^{abc}_{\rm shift}(\omega)$ for the zinc-blende crystals GaAs and GaP. For these crystals $\eta^{abc}_{\rm inj}(\omega)$ vanishes, and the electronic response to a continuous-wave laser consists of rectification and shift current contributions.

The wurtzite semiconductors are direct gap, noncentrosymmetric binary compounds, as are the zinc-blende semiconductors. However, the wurtzite crystal lattice belongs to the hexagonal crystal system; it is less symmetric than zinc-blende and has a more complicated primitive cell, consisting of four atoms instead of two. It belongs to the dihexagonal pyramidal crystal class 6mm, and space group $P6_3mc$ ($C6v4$). The orientation of the crystal is important in understanding the response. We use the coordinate system and basis convention as laid out in the text by Grosso and Parravacini.[25] The primitive lattice vectors are $\mathbf{t}_1 = a(1/2, \sqrt{3}/2, 0)$, $\mathbf{t}_2 = a(-1/2, \sqrt{3}/2, 0)$, and $\mathbf{t}_3 = c(0,0,1)$. The direction of $\mathbf{t}_3$ is called the c axis and is typically the growth axis. We use the empirical values $a = 8.126a_0$ and $c = 13.24a_0$. The Cd atoms are set at (0,0,0) and $(0, a/\sqrt{3}, c/2)$, and the S (or Se in CdSe) atoms are at $(0,0,uc)$ and $(0, a/\sqrt{3}, uc+c/2)$. For the internal parameter u, we use the ideal value $u = 3/8$.

We first discuss the symmetries of the optical susceptibility tensors of wurtzite. The linear optical response tensor $\chi^{ab}_1(-\omega;\omega)$ is diagonal in the frame used to identify the $\mathbf{t}_i$ above, but the low symmetry leads to $\chi^{xx}_1 = \chi^{yy}_1 \neq \chi^{zz}_1$. The second order nonlinear tensor $\chi^{abc}_2(-\omega_\Sigma;\omega_\alpha,\omega_\beta)$ tensor has the nonzero components: $\chi^{xzx}_2 = \chi^{yzy}_2$, $\chi^{xxz}_2 = \chi^{yyz}_2$, $\chi^{zxx}_2 = \chi^{zyy}_2$, and χ^{zzz}_2. Each of these components can be complex. However, the susceptibility tensors for the individual effects of optical rectification, shift current and injection current may have more symmetry constraints. Consider optical rectification: Using the reality of the polarization and intrinsic permutation symmetry, one has the additional constraint

$$\chi^{abc*}_{\rm rect}(\omega) = \chi^{acb}_{\rm rect}(\omega), \tag{44}$$

which naturally, our expression (35) satisfy; it follows from this that $\chi^{zzz}_{\rm rect}(\omega)$ and $\chi^{zxx}_{\rm rect}(\omega)$ are purely real. The xxz and xzx components are still complex but now they satisfy the additional relation $\chi^{xxz}_{\rm rect} = \chi^{xzx*}_{\rm rect}$.

These different tensor components can be accessed with different crystal orientations, and different polarizations of incident light. We consider one crystal orientation, in which the different tensor components can be accessed by different light polarizations. In this orientation, the light propagates along the $-\hat{\mathbf{y}}$ direction, and the laser electric field is polarized in the xz plane. This is a somewhat unconventional orientation, since for normal incidence it requires a crystal with the c axis lying in the plane of the surface. Most optical experiments on bulk wurtzite semiconductors, especially those involving absorption studies, use the xy plane as the sample surface, and have the light propagating along the c axis.

We consider four different excitation scenarios. In each we identify the polarization of the light in the crystal. This may differ slightly from the incident polarization but with the knowledge of the linear susceptibility the incident polarization could be adjusted to produce the desired polarization inside the crystal; in practice the adjustments would be small. We focus on the polarization state in the crystal to best demonstrate the various symmetry properties of the response.

In the first scenario, the light is linearly polarized along $\hat{\mathbf{z}}$ so that $\mathbf{E}_{\rm env}(t) = E_{\rm env}(t)\hat{\mathbf{z}}$. In this and the other scenarios, we assume the envelope functions $E_{\rm env}(t)$ are purely real. For this scenario, we expect an optical rectification polarization induced along $\hat{\mathbf{z}}$,

$$P^z_{\rm rect}(t) = 2\chi^{zzz}_{\rm rect}(\omega_0)E^2_{\rm env}(t). \tag{45}$$

For the second scenario, the light polarization is given by $\mathbf{E}_{\rm env}(t) = E_{\rm env}(t)\hat{\mathbf{x}}$, which also gives a rectification that is along $\hat{\mathbf{z}}$. This polarization is

$$P^z_{\rm rect}(t) = 2\chi^{zxx}_{\rm rect}(\omega_0)E^2_{\rm env}(t). \tag{46}$$

To access the component $\chi^{xxz}_{\rm rect}$, the light polarization must have components along $\hat{\mathbf{x}}$ and $\hat{\mathbf{z}}$. For the third scenario we consider light linearly polarized along $(\hat{\mathbf{x}}+\hat{\mathbf{z}})/\sqrt{2}$, so that $\mathbf{E}_{\rm env}(t) = E_{\rm env}(t)(\hat{\mathbf{x}}+\hat{\mathbf{z}})/\sqrt{2}$. This gives a rectification along $\hat{\mathbf{x}}$ of

$$P^x_{\rm rect}(t) = [\chi^{xzx}_{\rm rect}(\omega_0) + \chi^{xxz}_{\rm rect}(\omega_0)]E^2_{\rm env}(t). \tag{47}$$

It also gives a rectification along $\hat{\mathbf{z}}$, given by

$$P^z_{\rm rect}(t) = [\chi^{zzz}_{\rm rect}(\omega_0) + \chi^{zxx}_{\rm rect}(\omega_0)]E^2_{\rm env}(t). \tag{48}$$

Note that, from Eq. (44), the quantity in brackets in Eq. (47) is simply $2\,\mathrm{Re}[\chi^{xxz}_{\rm rect}(\omega_0)]$. To access the imaginary part of $\chi^{xxz}_{\rm rect}$, circularly polarized light can be used. For the fourth and final scenario, we consider $\mathbf{E}_{\rm env}(t) = E_{\rm env}(t)(\hat{\mathbf{x}}+i\hat{\mathbf{z}})/\sqrt{2}$, which gives

$$P^x_{\rm rect}(t) = i[\chi^{xxz}_{\rm rect}(\omega_0) - \chi^{xzx}_{\rm rect}(\omega_0)]E^2_{\rm env}(t). \tag{49}$$

The quantity $\chi^{xxz}_{\rm rect}(\omega_0) - \chi^{xzx}_{\rm rect}(\omega_0) = 2i\,\mathrm{Im}[\chi^{xxz}_{\rm rect}(\omega_0)]$ contains only terms that, at least within the independent particle model, vanish below the band gap. That is, this rectification polarization only exists for excitation at photon energies above the band-gap energy, and because such excitation is accompanied by absorption that leads to other processes generating strong currents, it would be difficult to distinguish the effects of this rectification polarization from those of other processes.

The different electric field polarizations in each scenario, and the induced optical rectification electric dipole polarizations, are summarized in Table I. We now turn to the shift and injection current processes. The shift current tensor $\sigma^{abc}_{\rm shift}(\omega)$ is purely real, and symmetric under exchange of b and c. Thus, there are three unique nonzero components: $\sigma^{zzz}_{\rm shift}$, $\sigma^{zxx}_{\rm shift} = \sigma^{zyy}_{\rm shift}$, and $\sigma^{xxz}_{\rm shift} = \sigma^{xzx}_{\rm shift} = \sigma^{yzy}_{\rm shift} = \sigma^{yyz}_{\rm shift}$. These tensor components can be accessed by using the same electric field

TABLE I. Summary of optically induced responses from different incident polarizations.

Polarization	Optical rectification	Shift current	Injection current
$E_{\rm env}(t)\hat{\mathbf{z}}$	$P^z_{\rm rect}(t)=2\chi^{zzz}_{\rm rect}(\omega_0)E^2_{\rm env}(t)$	$J^z_{\rm shift}(t)=2\sigma^{zzz}_{\rm shift}(\omega_0)E^2_{\rm env}(t)$	
$E_{\rm env}(t)\hat{\mathbf{x}}$	$P^z_{\rm rect}(t)=2\chi^{zxx}_{\rm rect}(\omega_0)E^2_{\rm env}(t)$	$J^z_{\rm shift}(t)=2\sigma^{zxx}_{\rm shift}(\omega_0)E^2_{\rm env}(t)$	
$E_{\rm env}(t)\frac{\hat{\mathbf{x}}+\hat{\mathbf{z}}}{\sqrt{2}}$	$P^x_{\rm rect}(t)=[\chi^{xzx}_{\rm rect}(\omega_0)+\chi^{xxz}_{\rm rect}(\omega_0)]E^2_{\rm env}(t)$	$J^x_{\rm shift}(t)=2\sigma^{xxz}_{\rm shift}(\omega_0)E^2_{\rm env}(t)$	
	$P^z_{\rm rect}(t)=[\chi^{zzz}_{\rm rect}(\omega_0)+\chi^{zxx}_{\rm rect}(\omega_0)]E^2_{\rm env}(t)$	$J^z_{\rm shift}(t)=[\sigma^{zzz}_{\rm shift}(\omega_0)+\sigma^{zxx}_{\rm shift}(\omega_0)]E^2_{\rm env}(t)$	
$E_{\rm env}(t)\frac{\hat{\mathbf{x}}+i\hat{\mathbf{z}}}{\sqrt{2}}$	$P^x_{\rm rect}(t)=i[\chi^{xxz}_{\rm rect}(\omega_0)-\chi^{xzx}_{\rm rect}(\omega_0)]E^2_{\rm env}(t)$	$J^z_{\rm shift}(t)=[\sigma^{zzz}_{\rm shift}(\omega_0)+\sigma^{zxx}_{\rm shift}(\omega_0)]E^2_{\rm env}(t)$	$\dot{J}^x_{\rm inj}(t)=2\eta^{xxz}_{\rm inj}(\omega_0)E^2_{\rm env}(t)$
	$P^z_{\rm rect}(t)=[\chi^{zzz}_{\rm rect}(\omega_0)+\chi^{zxx}_{\rm rect}(\omega_0)]E^2_{\rm env}(t)$		

polarizations as used above to investigate the rectification. In Table I we summarize the shift current responses from these different polarizations. In the fourth scenario, which involves circularly polarized light, there is no shift current along $\hat{\mathbf{x}}$, since $\sigma^{xxz}_{\rm shift}=\sigma^{xzx}_{\rm shift}$. In the continuous wave limit, it is common to introduce the shift distance $d^a_{\rm shift}$, defined as the average distance traversed by an electron as it is promoted from the valence band to the conduction band,

$$d^a_{\rm shift}=J^a_{\rm shift}/e\dot{n}, \tag{50}$$

where $\dot{n}$ is the carrier injection rate. In the continuous-wave regime, the carrier injection rate can be determined from Fermi's golden rule to be[26,27]

$$\dot{n}=\xi^{ab}(\omega)E^a(-\omega)E^a(\omega), \tag{51}$$

where the tensor $\xi^{ab}(\omega)$ is proportional to the linear response tensor $\chi^{ab}(-\omega;\omega)$, and is given by[27]

$$\xi^{ab}(\omega)=\frac{2\pi e^2}{\hbar}\int\frac{d^3k}{8\pi^3}\sum_{mn}f_{nm}r^a_{nm}r^b_{mn}\delta(\omega-\omega_{mn}). \tag{52}$$

There is only one unique nonzero component of the injection current susceptibility tensor,

$$\eta^{xxz}_{\rm inj}=-\eta^{xzx}_{\rm inj}=\eta^{yyz}_{\rm inj}=-\eta^{yzy}_{\rm inj}. \tag{53}$$

This tensor component can be accessed with circularly polarized light in which the superposed linear polarizations are along the c axis of the crystal and perpendicular to it. Using the circular polarization $(\hat{\mathbf{x}}+i\hat{\mathbf{z}})/2$, the resulting current injection rate is

$$\dot{J}^x_{\rm inj}(t)=2\eta^{xxz}_{\rm inj}(\omega_0)E^2_{\rm env}(t). \tag{54}$$

In the continuous-wave limit, we can use the swarm velocity $v_{\rm swarm}$ to characterize the injection current. The swarm velocity is defined as the average velocity of the injected electrons, and its component along a is given by

$$v^a_{\rm swarm}=\dot{J}^a_{\rm inj}/e\dot{n}. \tag{55}$$

B. CdS

We now evaluate the rectification, shift, and injection tensors using the expressions given in Sec. II. Our calculation of the band structure and matrix elements is done using density-functional theory, within the local-density approximation (LDA). We use the WIEN2K full-potential LAPW package to solve the Kohn-Sham equations and compute the matrix elements.[28] An all-electron approach is needed to account for the semicore states in CdS and CdSe. In the FLAPW approach the unit cell is partitioned into nonoverlapping atomic spheres centered at atomic sites, and an interstitial region. Spin-orbit interactions are included with a second variational step applied to the atomic sphere regions.[29] It is well known that the LDA underestimates the band gap. We find band-gap values of 1.41 eV and of 2.45 eV, for CdS and CdSe, respectively. For the calculation of the nonlinear response we use the scissors correction, as detailed by Nastos *et al.*[26] to adjust the band gap to the experimental values of 2.45 eV and 1.75 eV for CdS and CdSe, respectively. We follow the same computational details as in Nastos and Sipe,[19] so we refer the reader there for further details. For the Brillouin-zone integrations required to compute the response functions we use an adaptive integration scheme we have detailed elsewhere.[27]

In Figs. 1–3 we present the numerical result for the optical rectification susceptibility tensor $\chi^{abc}_{\rm rect}(\omega)$ as a function of electric photon energy $(\hbar\omega)$. In Fig. 1 we plot the real parts of the components $\chi^{zzz}_{\rm rect}(\omega)$, $\chi^{zxx}_{\rm rect}(\omega)$, and $\chi^{xxz}_{\rm rect}(\omega)$ for frequencies below the band gap, where there is no absorption. The component $\chi^{xxz}_{\rm rect}(\omega)$ is only real below the band gap, unlike $\chi^{zzz}_{\rm rect}(\omega)$ and $\chi^{zxx}_{\rm rect}(\omega)$, which are purely real at all frequencies. The static limit values are $\chi^{zzz}_{\rm rect}(0)=7.5$ pm/V and $\chi^{zxx}_{\rm rect}(0)=\chi^{xxz}_{\rm rect}(0)=-12.5$ pm/V. That $\chi^{zxx}_{\rm rect}(0)=\chi^{xxz}_{\rm rect}(0)$ reflects the full permutation symmetry at zero frequency (Kleinman symmetry).

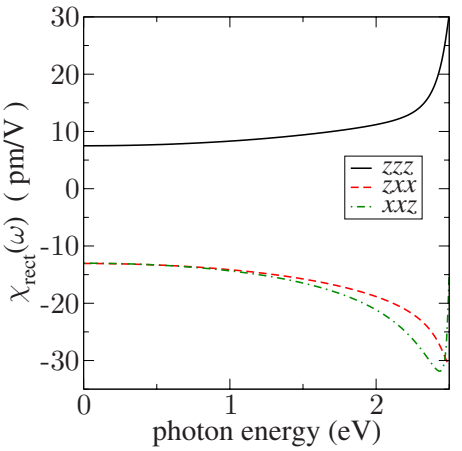

FIG. 1. (Color online) The optical rectification susceptibility tensor components $\chi^{zzz}_{\rm rect}$, $\chi^{zxx}_{\rm rect}$, and $\chi^{xxz}_{\rm rect}$ for CdS at laser photon energies below the band gap. The zzz and zxx components are purely real. The component xxz is purely real below the band gap.

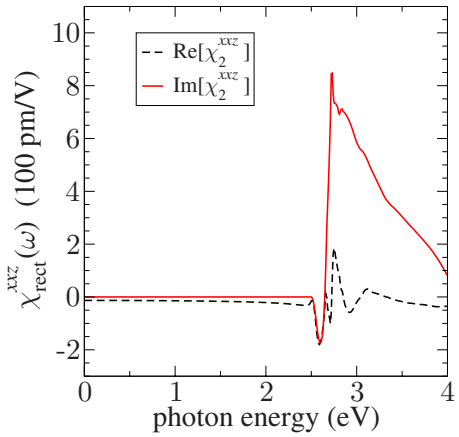

FIG. 2. (Color online) The real and imaginary parts of the optical rectification susceptibility component $\chi^{xxz}_{\rm rect}$ for CdS. The imaginary part is zero below the band gap.

In Figs. 2 and 3 we plot the real and imaginary parts of the component $\chi^{xxz}_{\rm rect}(\omega)$, and the components $\chi^{zzz}_{\rm rect}(\omega)$ and $\chi^{zxx}_{\rm rect}(\omega)$, over a much wider energy range. These results demonstrate that the response coefficient is much larger at photon energies above the band gap, where there are resonances due to absorption. Unfortunately, this strong absorption also leads to a small active region, which makes any conventional attempt to detect this coefficient above the band gap very difficult.

While there are a number of measurements and calculations of second-harmonic generation in bulk wurtzite crystals, we are unaware of any for the rectification response tensor $\chi^{abc}_{\rm rect}(\omega)$. Such measurements would in any case include lattice contributions to $\chi^{abc}_{\rm rect}(\omega)$ as well, which we have not calculated here. There is some merit in comparing our results to values of different χ_2 nonlinear effects. We expect these to be of the same order, since in the limit of zero frequency $\chi^{abc}(\omega_\Sigma;\omega_\alpha,\omega_\beta)\approx\chi^{abc}(0;\omega,-\omega)$ for the electronic response. The absolute values for the second-harmonic generation coefficients at low frequencies have been reported to be between 72 and 84 pm/V,[1] roughly a factor of 10 larger than our values; but these were very early measurements. In

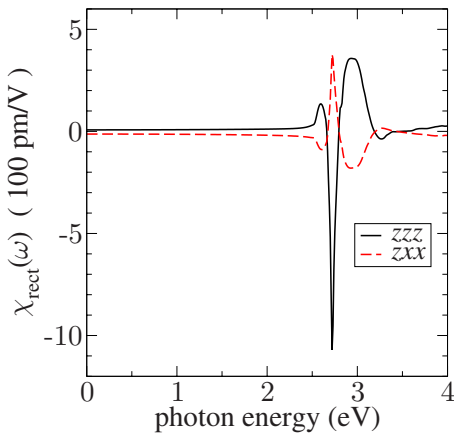

FIG. 3. (Color online) The CdS optical rectification susceptibility components *zzz* and *zxx* for photon energies below and above the band gap.

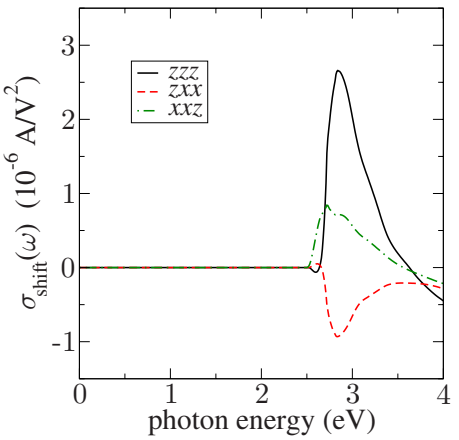

FIG. 4. (Color online) The shift current tensor σ^{zzz}, σ^{zxx}, and σ^{xxz} for CdS. Each component is zero below the band gap.

other theoretical work dealing with the second-order nonlinearity, Rashkeev and Lambrecht[30] reported the static limit of χ_2 to be 40 pm/V for *cubic* CdS, roughly a factor of four different from our results. While their calculation uses a similar approach to the LDA band structure as ours, the scissors correction they implemented is different. It is unclear how much of the difference could be due to that, or to other details of the calculations.

Note that the real and imaginary parts of $\chi^{xxz}_{\rm rect}(\omega)$ are not related by the Kramers-Kronig relation. This is borne out in Eq. (35). In this equation, the term $\chi^{abc}_{\rm 2inter}(\omega)$ satisfies the Kramers-Kronig relations but the real part $\Lambda^{abc}_{\rm I}(\omega)$ appears without its Kramers-Kronig pair $\Lambda^{abc}_{\rm II}(\omega)$. The $\Lambda^{abc}_{\rm II}(\omega)$ terms appear in the shift current [cf. Eq. (32)], to which we now turn.

In Fig. 4 we plot the three shift tensor components $\sigma^{zzz}_{\rm shift}(\omega)$, $\sigma^{zxx}_{\rm shift}(\omega)$, and $\sigma^{xxz}_{\rm shift}(\omega)$ as a function of photon energy. All three spectra are zero below the band gap, and they all attain a maximum absolute value within the first 0.5 eV above the band edge. The decrease at higher energies is because the participating states are from a larger area in the Brillouin zone, and the effective dipole moments with each final state are unaligned.

The shift currents in both wurtzite CdS and CdSe were experimentally investigated by Laman *et al.*[13] By measuring the THz radiation emitted from the shift current, they were able to extract the values $\sigma^{zzz}_{\rm shift}=8\times10^{-6}$ A/V^2 and $\sigma^{zxx}_{\rm shift}=3\times10^{-6}$ A/V^2 for CdS, at an excitation energy of roughly 3 eV. Our peak value near the band edge is no more than 3×10^{-6} A/V^2, which is within an order of magnitude of these experimental findings. For the *xxz* component we find worse agreement. The experiments of Laman *et al.* were unable to resolve a signal from this component, so they set an upper bound of 10^{-7} A/V^2. However, we find a sizeable nonzero component, comparable to the *zzz* and *zxx* component. Some of this discrepancy may be attributed to the surface of the crystal used in the experiments. To measure the *xxz* component in a THz emission experiment the crystal sample should be oriented with the *z* axis in the plane of the surface. This is a difficult crystal cut with which to work, since its surface is plagued with steps and other imperfec-

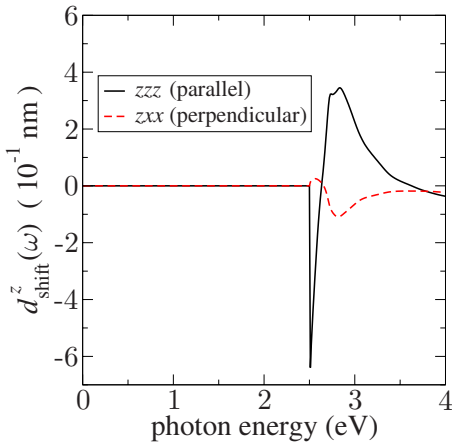

FIG. 5. (Color online) The shift distance d for CdS. The large variations arise from the different transitions that are excited near the band edge.

tions. A much smoother surface is obtained when the c axis is parallel to the growth axis. For completeness we note that for SHG the xxz component is of the same order of magnitude as the two components zzz and zxx.[1]

Turning now to the shift distance, we recall that in zinc-blende crystals the shift distance can be characterized by only one value, and a geometric factor accounting for the direction of the linear polarization of the light field.[19] In wurtzite crystals there are a number of combinations of optical polarizations and crystal orientations that give different values. For brevity, we only discuss two scenarios in which a shift current is excited along the c axis ($\hat{\mathbf{z}}$). In the first scenario the electric field is linearly polarized along $\hat{\mathbf{z}}$. We refer to as the "parallel" case. In the second scenario, which we refer to as the "perpendicular" case, the field is polarized along $\hat{\mathbf{x}}$. The shift distances $d^z_{\rm shift}$ are shown in Fig. 5. We see that for the parallel case the band edge the shift distance is almost 6 Å. This is roughly the unit cell c parameter, which is more than twice the bond length. At higher energies the shift distance changes sign and reaches almost 4 Å. This suggests that for some energies the above band-gap excitation leads to an electron transfer beyond the nearest neighbor. In the perpendicular case, where the electric field is not parallel to any bond, the shift distance is significantly smaller.

This picture of the shift distance in CdS is quite different than the model developed for GaAs. The intuition surrounding the shift distance for that material is that in the excitation process, the electron density makes transitions from the more electronegative ion to the less electronegative one. In a binary compound, there can be many multiple nearest neighbors that are less electronegative, and it is the electric field polarization that determines the direction, if any, of the net shift. For excitation just above the band gap in GaAs, we have found that the shift distance is approximately the bond length.[19] At higher energies the shift distance varies in a range between the bond length to half the bond length. This leads to an interpretation in which the transfer occurs only between nearest neighbors for a wide range of energies. From the calculations presented here, this picture breaks down for the wurtzite materials. One approach to understand the underlying microscopic dynamics driving the shift current is to calculate the evolution of the microscopic current and charge densities as a function of time under the influence of the laser field but this is beyond the scope of the current work.

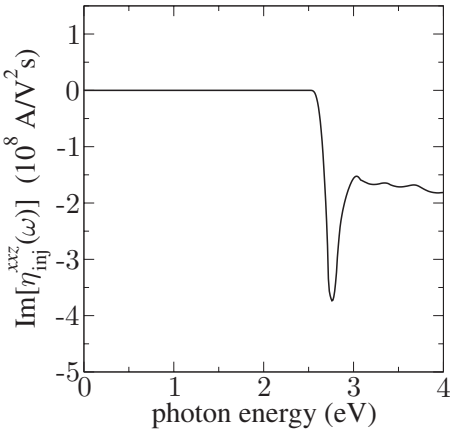

FIG. 6. The imaginary part of the injection current susceptibility tensor component $\eta^{xxz}_{\rm inj}$ for CdS. The components $\eta^{xxz}_{\rm inj}=\eta^{yyz}_{\rm inj}=-\eta^{xzx}_{\rm inj}=-\eta^{yzy}_{\rm inj}$ are the only nonvanishing components. All components are zero below the band gap. The variation near the band edge is from the transitions from crystal-field and spin-orbit split levels to the conduction band.

Finally, we turn to the injection current tensor $\eta^{xxz}_{\rm inj}$. In Fig. 6 we plot the imaginary part of the component $\eta^{xxz}_{\rm inj}$. Like the shift current tensor, the injection current tensor is zero below the band gap. Above the band gap, the tensor is purely imaginary and achieves its maximum value at a photon energy of approximately 2.75 eV, just above the band gap. The large variation as a function of photon energy is attributed to the crystal-field and spin-orbit splittings in the valence bands. This is clearer when considering the swarm velocity, which is the average speed of the injected carriers. In Fig. 7 we plot the swarm velocity for the scenario in which the light is circularly polarized along $(\hat{\mathbf{x}}+i\hat{\mathbf{z}})/2$. The swarm velocity

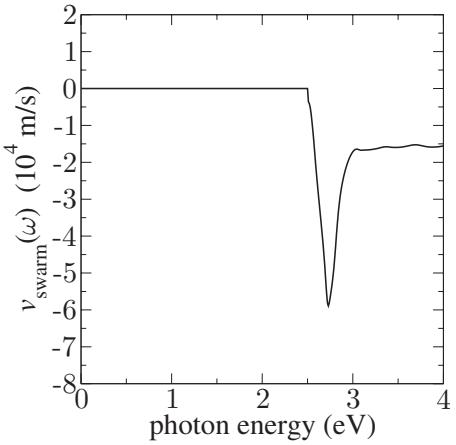

FIG. 7. The swarm velocity $v_{\rm swarm}$ for CdS, as defined in the text. The peak swarm velocity is almost 60 km/s, attained at excitation energies of around 2.7 eV just above the transition energy from the split-off band energy (2.57 eV).

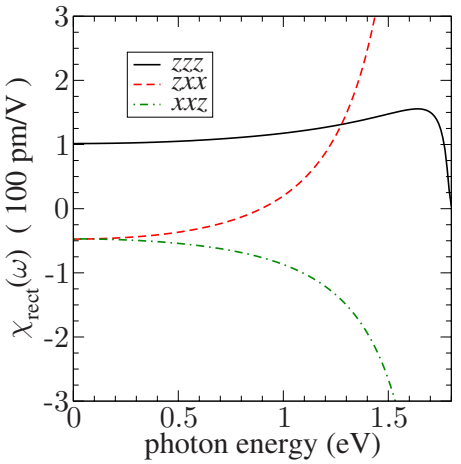

FIG. 8. (Color online) The optical rectification susceptibility components $\chi^{zzz}_{\rm rect}$, $\chi^{zxx}_{\rm rect}$, and $\chi^{xxz}_{\rm rect}$ for CdSe. The *zzz* and *zxx* components are purely real at all frequencies. The *xxz* component is only real below the band gap.

spectrum has roughly the same profile as the injection current, except that the onset at the band edge and the variation around the peak value are a little more abrupt. The peak swarm velocity appears at photon energies well above the band edge but below the split-off energy. This is because the electron group velocities become larger at higher energies in the band structure near the Γ point, but once the energies exceed the split-off band the large volume of states participating in the response make the crystal effectively more symmetric in its response to the laser light; for high symmetry crystals, such as zincblende GaAs, the injection current vanishes. Laman *et al.* could not measure the phase of the current injection tensor, but found it had a magnitude of approximately $4i\times10^8$ A/V^2 s at a photon energy of 3.0 eV. At this photon energy we calculate a value of about $1.6i\times10^8$ A/V^2 s. However, there is much variation in the spectrum in the neighborhood of this photon energy, and given the errors in the curvature of the LDA bands near the gap, it is unrealistic to compare the response at a particular frequency. Our peak magnitude near the band edge is about $3.8i\times10^8$ A/V^2 s which is closer to peak value seen by Laman *et al.*

The average injected velocity of the electrons, the swarm velocity $v_{\rm swarm}$, is shown in Fig. 7. Like the injection current, the spectrum has a sharp peak at photon energies above the band edge, and drops off rapidly above the split-off energy. We find a maximum swarm velocity magnitude of about 60 km/s at about 2.7 eV excitation. Laman *et al.* determined a swarm velocity of 20 km/s at 3.0 eV. At the same photon energy we find a magnitude of around 18 km/s, in very close agreement.

C. CdSe

We turn to the results for CdSe. In Figs. 8 and 9 we plot the rectification tensor components *zzz*, *zxx*, and *xxz*. The spectra for CdSe show some striking differences from the CdS results. In particular, the resonances from the band gap,

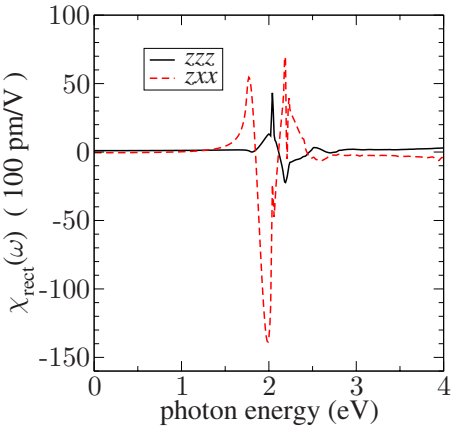

FIG. 9. (Color online) The optical rectification susceptibility components $\chi^{zzz}_{\rm rect}$ and $\chi^{zxx}_{\rm rect}$ for CdSe at frequencies below and above the band gap.

at 1.75 eV, cause large variations in the rectification below the gap. Indeed, for the *zxx* component, our calculations indicate that the variation is strong enough to lead to a sign change.

We are unaware of any other calculations of the rectification tensor for CdSe. For cubic CdSe, however, calculations of the second-harmonic response coefficient in the static limit have been reported. Rashkeev and Lambrecht[30] find a static limit of 50 pm/V. However, they did not find a resonance effect as striking as ours. Dal Corso *et al.*[31] found a larger value of $\chi_2=118$ pm/V for cubic CdSe. For wurtzite CdSe, Roberts has reported experimental values for the low-frequency second-harmonic response.[32] He found $\chi^{zzz}=72$ pm/V, and $\chi^{xxz}=-36$ pm/V at a wavelength of 10.6 μm. Although it is difficult to make an exact comparison, our results for the static limit ($\chi_2^{zzz}=102$ pm/V and $\chi_2^{zxx}=\chi_2^{xxz}=-48$ pm/V) are within a factor of 2 of these results. This is very good agreement, given the complications of comparing the static limit of these two effects. Turning to the shift current in CdSe, in Fig. 10 we present the shift current tensor components.

We find that all three components are large and have peak magnitudes in the range of $4\times10^{-6}-18\times10^{-6}$ A/V^2. While

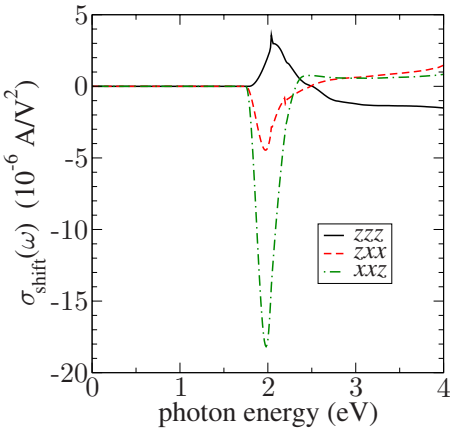

FIG. 10. (Color online) Shift current susceptibility tensor of CdSe. All components of the tensor vanish at energies below the band gap.

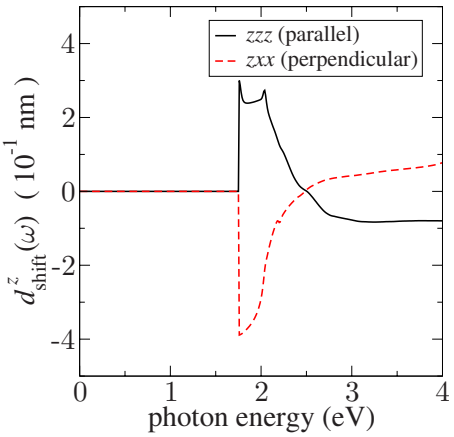

FIG. 11. (Color online) Shift distance in CdSe. The large variations arise from the different transitions that are excited near the band edge. At energies well above the split-off energy, the shift distance is very small.

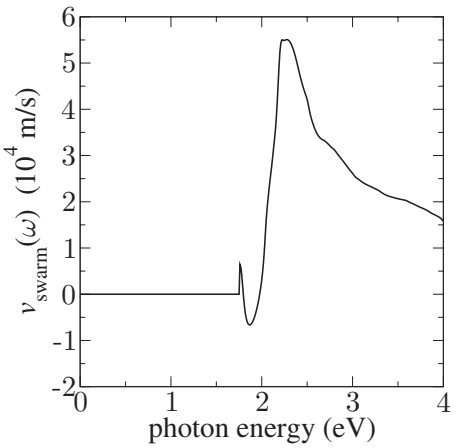

FIG. 13. The swarm velocity of CdSe, as defined in the text. The peak swarm velocity is approximately 55 km/s at 2.2 eV, which is just above the transition energy from the split-off band energy.

the *zzz* and *zxx* components are of the same order of magnitude as found by Laman *et al.* we again find a much larger *xxz* component, which was undetected in their experiments.

In Fig. 11 we plot the shift distance for the parallel and perpendicular cases of linearly polarized light, as described in the CdS section. At the band edge, the shift distance in the parallel orientation is roughly equal to the CdSe bond length (0.27 nm). This is similar to the situation in GaAs, where we found that the shift distance was also very near the bond length. The perpendicular orientation, however, has a shift distance that is almost twice the bond length. Laman *et al.* determined an experimental value of 0.1 nm for CdSe, almost a factor of 3 smaller than what we find. Finally, we turn to the injection current. In Fig. 12 we plot the injection current susceptibility.

The variation near the turn on at 1.75 eV is due to the crystal-field splitting and spin-orbit coupling. At the onset, the component is actually positive for about two tens of an electron volt, and then turns negative when the photon energy crosses the crystal-field splitting energy. It then stays negative up to an energy corresponding to the spin-orbit coupling, at which point it turns positive at about 2.25 eV. At this energy the split-off bands participate in the excitation process, and this leads to a smaller injection current. Comparing to experiment, Laman *et al.* found an experimental value of approximately 1.5×10^8 A/V^2 s at a photon energy of 1.80 eV. At 1.8 eV we find a value of under 0.5×10^8 A/V^2 s. The swarm velocity $v_{\rm swarm}$, for CdSe is shown in Fig. 13. The effect of the crystal-field splitting is more pronounced here than for CdS. The swarm velocity is positive near the band edge, and turns negative once the crystal-field split states participate. As the energy increases the split-off bands participate causing the sign to change again. At 2.2 eV we find the maximum swarm velocity for CdSe of about 50 km/s. At higher photon energies the crystal effectively appears more symmetric to the laser light, and the injection current begins to vanish. Laman *et al.* estimated a swarm velocity of 9 km/s at 1.80 eV. Our theoretical calculations predict roughly 8 km/s at that photon energy, in good agreement with their measurement.

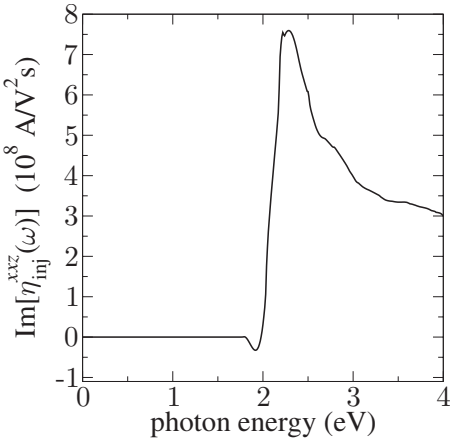

FIG. 12. The imaginary part of the injection current susceptibility tensor component $\eta^{xxz}_{\rm inj}$ for CdSe. The components $\eta^{xxz}_{\rm inj}=\eta^{yyz}_{\rm inj}=-\eta^{xzx}_{\rm inj}=-\eta^{yzy}_{\rm inj}$ are the only nonvanishing components. All components are zero below the band gap. The variation near the band edge is from the transitions from crystal-field and spin-orbit split levels to the conduction band.

IV. CONCLUSIONS

Under pulsed excitations, the near-dc second-order response of semiconductors can be understood to be dominated by three current responses: optical rectification, shift, and injection current. We have generalized our earlier treatment of this response to arbitrary crystal class. The approach clearly identifies the shift and injection currents within the second-order response, and also identifies a divergence-free expression for the optical rectification tensor $\chi^{abc}_{\rm 2rect}(\omega)$ applicable to clean, cold, semiconductors of any crystal class, both below and above the band gap.

We have applied the formalism to calculate the optical rectification, shift and injection current tensors in wurtzite CdS and CdSe within an FLAPW approach. For the static limit our results for CdSe are within a factor of 2 of results taken from SHG measurements. Our comparison of our re-

sults with a more recent experiment by Laman *et al.*,[13] investigating the shift and injection currents in CdSe and CdS, shows larger differences. While we find reasonable agreement for effects associated with the *zzz* and *zxx* components of the shift current tensor, we predict an equally strong *xzx* component, while Laman *et al.* could not resolve this component. These measurements are difficult and we hope that these theoretical results will encourage more experimental studies.

The calculations utilize the scissors correction to correct for the underestimation of the band gap typical in band structures calculated from density functional theory within the LDA. However, the scissors correction only provides a rigid shift of the conduction bands upward to higher energies, and cannot be expected to provide correct effective masses near the band gap. The curvature of the bands there will thus be incorrect, and calculations of optical quantities very near the gap will be affected. We do not expect that the scissors correction would work as well for materials such as CdS and CdSe as it would for GaAs and Si, where the shifts lead to smaller relative corrections to the band gaps. Part of the disagreement between theory and experiment may be due to this as well, and we hope our results will encourage more sophisticated theoretical studies.

ACKNOWLEDGMENTS

This work was supported by the Natural Sciences and Engineering Research Council of Canada and Photonics Research Ontario. We thank H. M. van Driel and N. Laman for discussions and comments.

APPENDIX: DERIVATION OF Eq. (24)

Here we derive the identity $\Gamma^{abc'}(\omega)=\Lambda^{abc}(\omega)-\Lambda^{acb}(\omega)$. From (the discussion around Eq. (18) of) Ref. 19 we have,

$$\Gamma^{abc}(\omega_\beta) = -\frac{ie^3}{8\hbar^2}\int \frac{d^3k}{8\pi^3}\sum_{mn} \Delta^a_{mn} f_{nm}[r^c_{nm}, r^b_{mn}]F_+(\omega_{mn},\omega_\beta), \tag{A1}$$

where

$$F_\pm(\omega_{mn},\omega) = \frac{1}{\omega_{mn}-\omega-i\eta} \pm \frac{1}{\omega_{mn}+\omega+i\eta}. \tag{A2}$$

Now consider $\Gamma^{abc'}(\omega)$. To evaluate this, we use

$$\frac{\partial}{\partial\omega}F_+(\omega_{mn},\omega) = -\frac{\partial}{\partial\omega_{mn}}F_-(\omega_{mn},\omega) \tag{A3}$$

and

$$\Delta^a_{mn}\frac{\partial}{\partial\omega_{mn}} = \frac{\partial}{\partial k^a}, \tag{A4}$$

and integrate by parts. Using

$$\frac{\partial}{\partial k^a}[r^c_{nm}, r^b_{mn}] = r^c_{nm;a}r^b_{mn} + r^c_{nm}r^b_{mn;a} - r^b_{nm;a}r^c_{mn} - r^b_{nm}r^c_{mn;a}, \tag{A5}$$

we get

$$\Gamma^{abc'}(\omega) = -\frac{ie^3}{8\hbar^2}\int \frac{d^3k}{8\pi^3}\sum_{mn} f_{nm}(r^c_{nm;a}r^b_{mn} + r^c_{nm}r^b_{mn;a} - r^b_{nm;a}r^c_{mn} - r^b_{nm}r^c_{mn;a})F_-(\omega_{mn},\omega). \tag{A6}$$

Now using

$$r^c_{nm}(-\mathbf{k})r^b_{mn;a}(-\mathbf{k}) = -r^c_{mn}(\mathbf{k})r^b_{nm;a}(\mathbf{k}), \tag{A7}$$

and noting that we can take $-\mathbf{k}\to\mathbf{k}$ under the integral, we get

$$\Gamma^{abc'}(\omega) = -\frac{ie^3}{4\hbar^2}\int \frac{d^3k}{8\pi^3}\sum_{mn} f_{nm}(r^b_{mn}r^c_{nm;a} - r^c_{mn}r^b_{nm;a})F_-(\omega_{mn},\omega). \tag{A8}$$

But $\Lambda^{abc}(\omega)$ is given by

$$\Lambda^{abc}(\omega) = -\frac{ie^3}{4\hbar^2}\int \frac{d^3k}{8\pi^3}\sum_{mn} f_{nm}r^b_{mn}r^c_{nm;a}F_-(\omega_{mn}-\omega), \tag{A9}$$

which gives us Eq. (26). We have verified that this numerically holds over the photon energy range 0–4 eV.

[1] R. W. Boyd, *Nonlinear Optics* (Academic Press, San Diego, 1992).
[2] J. A. Armstrong, N. Bloembergen, J. Ducuing, and P. S. Pershan, Phys. Rev. **127**, 1918 (1962).
[3] C. Aversa and J. E. Sipe, Phys. Rev. B **52**, 14636 (1995).
[4] D. E. Aspnes, Phys. Rev. B **6**, 4648 (1972).
[5] E. Ghahramani, D. J. Moss, and J. E. Sipe, Phys. Rev. B **43**, 8990 (1991).
[6] E. I. Blount, Solid State Phys. **13**, 305 (1962).
[7] R. von Baltz and W. Kraut, Phys. Rev. B **23**, 5590 (1981).
[8] R. von Baltz in *Ultrafast Dynamics of Quantum Systems: Physical Processes and Spectroscopic Techniques*, Nato Advanced Studies Institute Series B Vol. 372, edited by B. Di Bartolo (Plenum, New York, 1998).
[9] J. B. Khurgin, J. Opt. Soc. Am. B **11**, 2492 (1994).
[10] D. Côté, N. Laman, and H. M. van Driel, Appl. Phys. Lett. **80**, 905 (2002).
[11] R. Adomavičius, G. Molis, A. Krotkus, and V. Sirutkaitis, Appl. Phys. Lett. **87**, 261101 (2005).
[12] M. Bieler, K. Pierz, U. Siegner, and P. Dawson, Phys. Rev. B **76**, 161304(R) (2007).
[13] N. Laman, M. Bieler, and H. M. van Driel, J. Appl. Phys. **98**, 103507 (2005).
[14] N. Laman, A. I. Shkrebtii, J. E. Sipe, and H. M. van Driel, Appl. Phys. Lett. **75**, 2581 (1999).
[15] S. D. Ganichev and W. Prettl, J. Phys.: Condens. Matter **15**, R935 (2003).
[16] M. Bieler, N. Laman, H. M. van Driel, and A. L. Smirl, Appl.

Phys. Lett. **86**, 061102 (2005).
[17] M. Bieler, K. Pierz, and U. Siegner, J. Appl. Phys. **100**, 083710 (2006).
[18] J. E. Sipe and A. I. Shkrebtii, Phys. Rev. B **61**, 5337 (2000).
[19] F. Nastos and J. E. Sipe, Phys. Rev. B **74**, 035201 (2006).
[20] M. Bass, P. A. Franken, J. F. Ward, and G. Weinrich, Phys. Rev. Lett. **9**, 446 (1962).
[21] M. Bass, P. A. Franken, and J. F. Ward, Phys. Rev. **138**, A534 (1965).
[22] J. F. Ward, Phys. Rev. **143**, 569 (1966).
[23] X. C. Zhang, Y. Jin, K. Yang, and L. J. Schowalter, Phys. Rev. Lett. **69**, 2303 (1992).
[24] Gaussian units are used in the expressions throughout the paper. However, the figure plots of the spectra are presented in SI-MKS.
[25] G. Grosso and G. P. Parravacini, *Solid State Physics* (Academic Press, New York, 2000).
[26] F. Nastos, B. Olejnik, K. Schwarz, and J. E. Sipe, Phys. Rev. B **72**, 045223 (2005).
[27] F. Nastos, J. Rioux, M. Strimas-Mackey, B. S. Mendoza, and J. E. Sipe, Phys. Rev. B **76**, 205113 (2007).
[28] P. Blaha, K. Schwarz, G. K. H. Madsen, D. Kvasnicka, and J. Luitz, in *WIEN2k, An Augmented Plane Wave + Local Orbitals Program for Calculating Crystal Properties*, edited by K. Schwarz (Technische Universität Wien, Austria, 2001).
[29] A. H. MacDonald, W. E. Pickett, and D. D. Koelling, J. Phys. C **13**, 2675 (1980).
[30] S. N. Rashkeev and W. R. L. Lambrecht, Phys. Rev. B **63**, 165212 (2001).
[31] A. Dal Corso, F. Mauri, and A. Rubio, Phys. Rev. B **53**, 15638 (1996).
[32] D. A. Roberts, IEEE J. Quantum Electron. **28**, 2057 (1992).